Iranian Journal of Science & Technology, Transaction B, Engineering, Vol. 30, No. B3
Printed in The Islamic Republic of Iran, 2006

ELABORATION CONDITIONS, MICROSTRUCTURE AND PROPERTIES RELATIONSHIP IN SILICIUM NITRIDE CERAMICS*

M. KALANTAR[1**] AND G. FANTOZZI[2]

[1]Dept. of Materials Engineering, Yazd University, Yazd, I. R. of Iran
Email: mkalantar@yazduni.ac.ir
[2]INSA GEMPPM, URA 341, 69621 Villeurbanne Cedex, France

Abstract– Silicium-Based Ceramics were investigated to determine the effect of microstructural parameters and densification on thermal stress resistance to fracture initiation during thermal shock testing. The different materials and microstructures were obtained by changing parameters such as the type of powder, additive, forming process and sintering condition. Critical temperature differences (ΔT_c), after water quenching, are discussed in relation to change in Young's module of elasticity, a variable affecting thermal shock. The maximum thermal shock resistance of dense Si_3N_4 has been achieved after completing conversion $\alpha \rightarrow \beta$, the changes in grain morphology toward elongated grain and the relative crystallisation of the second phase. These characteristics are produced by a higher percentage of the powder in the α-phase, high Y_2O_3, and the sintering condition at a higher temperature (2000°C), longer soaking times (1h) and load application at the beginning of thermal cycle.

Keywords– Non-oxide ceramics, sintering, microstructure, mechanical properties, silicon nitride

1. INTRODUCTION

Improved Ceramic Materials have been developed for use in cases of rapidly changing temperature. The quality of these materials is generally evaluated by the measurement of crack resistance or toughness behavior upon crack extension, namely R or K_R –curve behavior, and thermal shock properties. Thermal shock strength degradation problems are still one of the major limitations of ceramics for many high temperature applications. Dens Silicium–Nitride Ceramics having a covalent bond can be resistant to transient thermal stresses during thermal shock processing due to its low coefficient of thermal expansion, moderate elastic modulus, high fracture toughness and relatively good resistance to oxidation compared to other high-temperature structural materials [1, 2]. Moreover, the lower density of these ceramics, about 40% of the density of high temperature superalloy, may offer components of lower weight and, therefore is sometimes an important advantage over other high-temperature materials. The high fracture toughness is a result of a fibrous microstructure which develops during fabrication [3-5], if the initial powder has the proper characteristics and the fabrication procedure can be controlled [6-16]. Literature generally agrees on the point that thermal shock resistance to fracture initiation of ceramics is controlled by the changes in mechanical and thermophysical properties which are strongly influenced by grain morphology, overall grain size, phase composition and the amount of the glassy phase [17-23]. The purpose of this investigation is to use different origin powders and to optimize processing conditions to obtain microstructural development and properties in relation with high temperature applications. Consequently we will develop different microstructures.

*Received by the editors June 29, 2005; final revised form May 1, 2006.
**Corresponding author

2. EXPERIMENTAL PROCEDURE

a) Starting material

The main characteristics of the commercial Silicon Nitride powders (M11, SN-E10 and S.H.S, SNE05) are given in Table 1. Different ratios of Y_2O_3 and Alumina have been added to the Silicon Nitride as sintering aids [24-28].

Table 1. Physicochemical characteristics of Si_3N_4 powders

	M11	SN-E10	SN-E05	S.H.S
Average particle size (μm):	0.7	0.45	0.7	0.5
Specific surface area(m^2/g):	10-13	10	4-6	10-15
Phase composition (%α):	≥90%	≥95	≥97	>90%
Green density (g/cm^3):	3.14	3.12	3.16	3.13
Morphology	plate	equiaxe	equiaxe	plate
Chemical composition (w%):	1.4	<2	1.08	<0.2
O		<100	<100 ppm	
Cl:	0.2	ppm	-	<0.1
C:	0.01		<100 ppm	<0.15
Fe:	0.08	<100pp	<50ppm	
Al:	0.01	m	<50ppm	
Ca:		<50ppm		
		<50ppm		

b) Materials preparation

The processing of the powders is schematically described in Fig. 1. Different processing conditions have been investigated (Table 2).

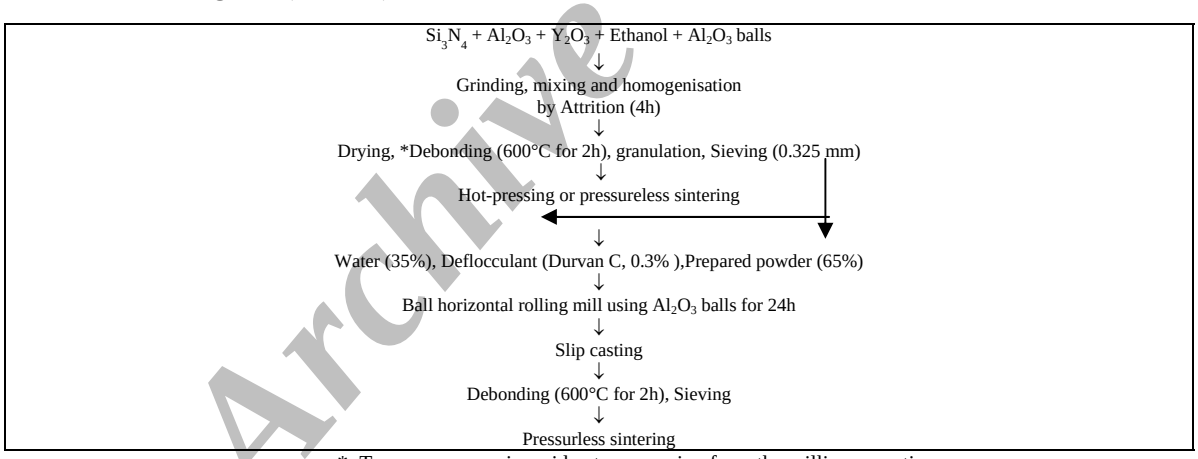

*: To remove organic residue trace coming from the milling operation

Fig. 1. Flow chart diagram of the material preparation

c) Materials characterisation

The disc shaped sintered specimens were cut into bar shape samples with a dimension of 3×4×25 mm (Fig. 2). The bar was subsequently polished down to 1 μm diamond paste.

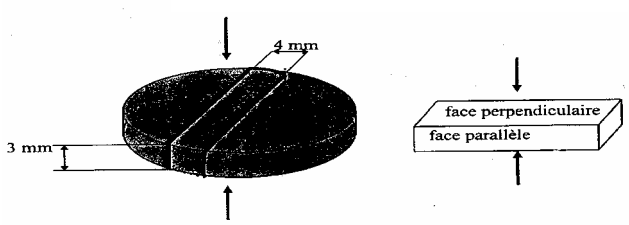

Fig. 2. Disc shaped sintered specimens and cut to bar shape samples

The microstructure was revealed by the microwave plasma etching technique (150 W, 2.54 GHz, Hydrogen pressure 2 kPa, 600°C, 10h) [29] and was observed by SEM (JEOL, Jsm 840A, LGS: Philips X(20) after metallization. Microstructure of fracture surface was also observed in order to evaluate the failure origins.

The strength was measured by a 4-point bending test (inner and outer span: 10-21 mm).The toughness was measured by controlled propagation of Vickers cracks. For this purpose, Vickers indentations were made with a load of 100N on the tensile surface of a bend specimen. In order to observe and measure the crack lengths under a traveling microscopy, the specimens were polished to 3 μm with a diamond paste. The specimens were single-edge notched to relative crack lengths of $a/w \geq 0.65$ with diamond blade of about 70 μm thickness. The loading was applied at a constant displacement rate to achieve the controlled – crack growth in three-point bending with a span length of 30 mm, done with a servo-hydraulic tension/compression testing machine (RM 25T Schenk-Trebel). Using the load –displacement curves, HPSN Ceramic materials, can be evaluated, the procedure has been described elsewhere [30, 31]. The Vickers hardness has been measured by means of a 10 N load. The Young's modulus has been measured by recording the resonance frequency in bending using a grindosonic apparatus. Thermal shock test was conducted by heating a bar shaped specimen in an electric furnace followed by water quenching. The thermal shock resistance has been evaluated by recording the evolution of dynamic Young's modulus after increasing temperature differences. The temperature at which a sudden fall of Young's modulus occurs was defined as the critical temperature difference (ΔT_c). Bulk density was measured by the archimed technique.

Table 2. The different processing conditions

N°	sintering condition				
Sample	Temperature (°C)	Time (min)	Fabrication technique	Atmosphere	Composition of powder
R1	1700	60	HP: Hot-pressed at 45 MPa, at T_d[1]	Ar	M11+A
R2	1800	"	"	"	"
R3	1700	"	"	N_2	"
R4	1800	″	"	"	″
R5	2000	"	"	"	″
R6	1800	"	"	"	M11+B
R7	2100	"	"	"	"
R8	2100	"	"	"	M11+ C
R9	1800	20	45 MPa at T_i[2]	"	M11 + A
R10	"	40	"	"	"
R11	"	60	"	"	"
R12	2000	″	″	"	"
R13	1800	″	SC + PS[3]	"	"
R14	″	″	CP + PS[4]	"	"
R16	1800	60	HP	"	SN-E10 + A
R17	2000	"	"	"	"
R18	2000	90	"	"	"
R19	1800	60	"	"	SNE05+A
R20	1800	"	SC + PS		SNE05+A
R20a	1800	60	Ref. 20 + HIP[5]	"	SNE05+A
R21	2000	60	HP	"	S.H.S + A
R22	"	90	"	"	"

A: 8%Y_2O_3, 1.5%Al_2O_3; B: 14% Y_2O_3, 1.5% Al_2O_3; C: 14% Y_2O_3, 4% Al_2O_3

1: Load applied at the beginning of dwell thermal cycle 2: Load applied at the beginning of thermal cycle 3: Slip Casting plus pressureless Sintering 4-Cold Pressing plus Pressureless sintering 5: Hot Isostatic Pressing

3. RESULTS AND DISCUSSION

The main physical and mechanical characteristics of the prepared samples are shown in Table 3 and the SEM microstructures are represented in Fig. 3.

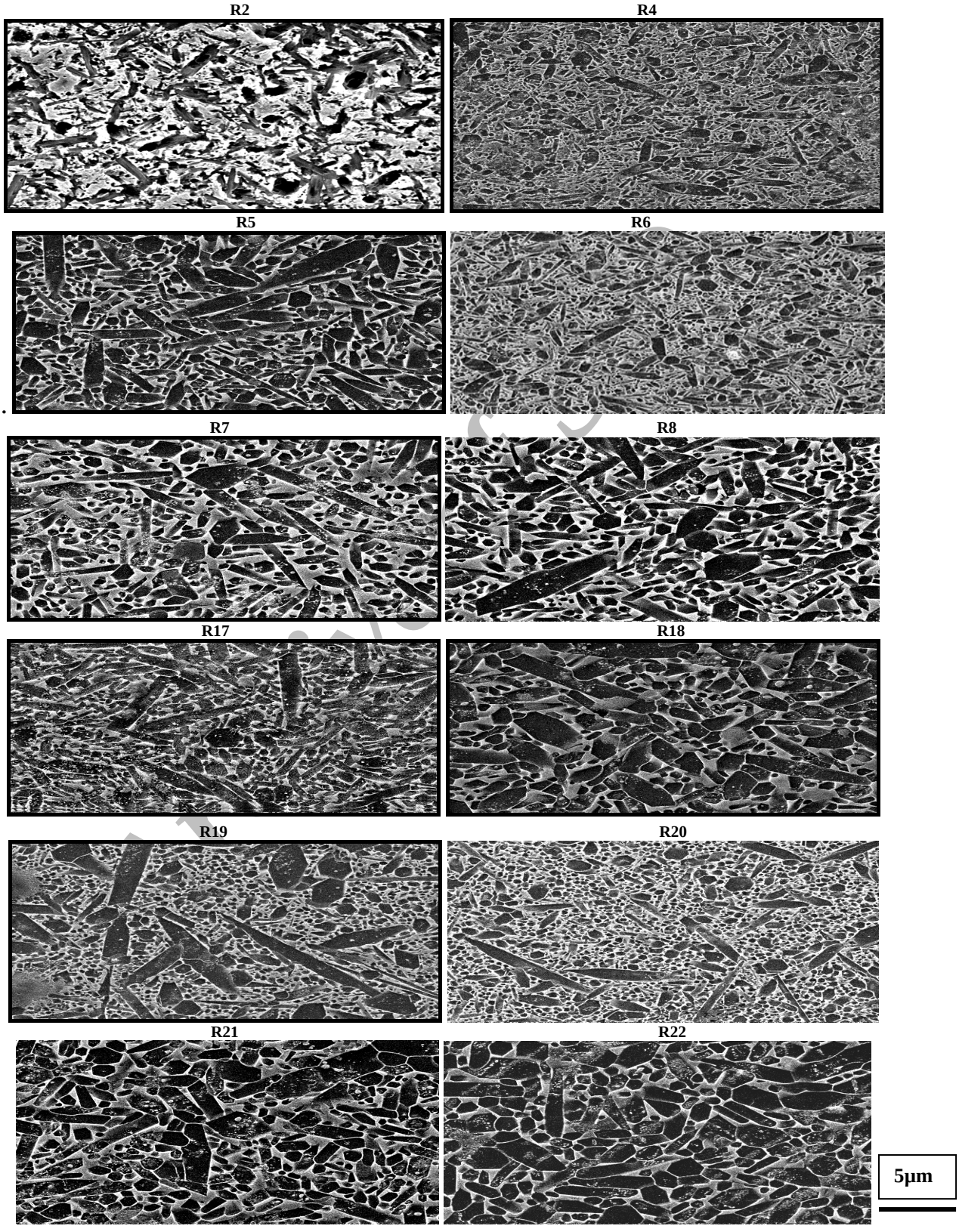

Fig. 3. Grain morphology of different prepared sample

Table 3. The sintered sample characteristics

Ref.	D(g/cm3)	E (GPa)	HV10 (GPa)	σ_f (MPa)	K_{IC} (MPa.m$^{1/2}$)	ΔT (K)
R1	3.19	279	14.59	638	-	480
R2	3.19	282	14	490	5.8	500
R3	3.25	306	16.28	806	7	550
R4	3.26	304	15.67	840	8	605
R5	3.25	311	14.57	780	10	800
R6	3.34	306	14.44	523	7.75	530
R7	3.32	311	14.71	758	9.5	850
R8	3.33	316.5	14.39	657	-	770
R9	3.25	311	14.44	582	6	380
R10	3.28	314	14.65	602	8.5	-
R11	3.27	321	14.75	800	10	-
R12	3.27	312	14.8	860	10.25	800
R13	3.26	324	14.3	755	10	650
R14	3.14	274.4	13	413	-	-
R16	3.27	327	14.9	840	9	550
R17	3.25	313	15.63	860	10	870
R18	3.3	320	15.3	800	11	1000
R19	3.25	313	14.29	700	9.8	690
R20	3.25	327	14.17	714	9.4	600
R20a	3.27	335	-	800	6	630
R21	3.23	300	14	694	7.6	650
R22	3.26	304	14	600	8.7	670

a) Properties of the starting powder

Among different powders (SN-E10, SN-E05, M11, SHS), SN-E10 shows the higher densification, mechanical properties and thermal shock resistance (Fig. 4a, b). The high percentage of the α-phase (≥97%), the equiaxial particle morphology and low amounts of the impurities for the SN-E10 enhance the formation of rod-like β-grains. The resulting aspect ratio of the elongated β-grains as a function of the %α-phase in the starting powder which is described in the literature as: a = 1+ α/β [10] is presented in Fig. 5. The powder M11 contains a large number of β- particles (Table 1) that cause the dissolution of the fine particles due to their higher chemical potential. The dissolved species continuously precipitate on the coarser original β- particles under a nearly equilibrium condition in such a way that their surface energy is minimised. This leads to the microstructure consisting of β-grains with lower aspect ratios associated with larger grain sizes and lower properties. The powders S.H.S, in relation to others, results in a considerable decrease of the densification and the mechanical properties. The microstructure of the hot pressed sample of this powder shows the large spherical or equiaxed grains that can be due to the large amount of β-phase present in the starting powder. Figure 3 shows the microstructures of different powders sintered in the same conditions (R5, R17, R21).

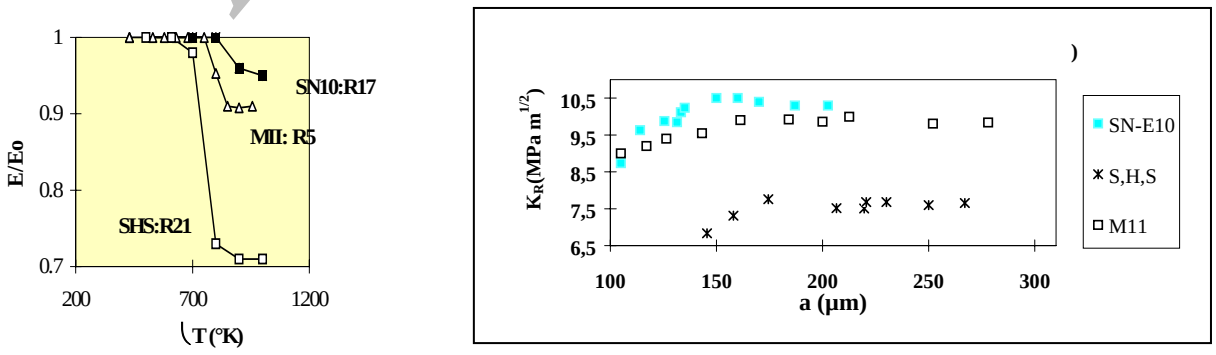

(a) (b)

Fig. 4. a) Young's modulus (RT) as a function of quenching temperature difference after water quench (22°C) for M11, SN-E10, SN-E05 materials, b) R-curve for sintered materials by different powders

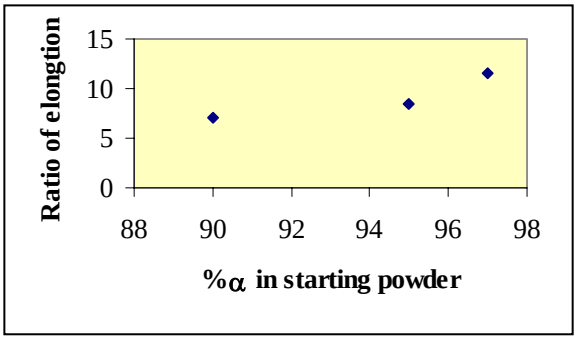

Fig. 5. Ratio of elongation according to initial amount of phase α in starting powder

b) Type and amount of sintering additives

Adding a higher Y_2O_3 concentration at low temperature (1800°C) decreases the sinterability, and consequently, densification and the mechanical properties (Table 3: R4, R6). Therefore, it is necessary to increase the sintering temperature to obtain a high aspect ratio of the precipitated β- Si_3N_4 grains (Fig. 3: R6, R7) and to improve mechanical properties and thermal shock resistance. In fact, a slow reduction of local supersaturation by high viscosity melts (meaning low diffusion rates) crystallise the grains of very high aspect ratios after spontaneous nucleation and promotes idiomorphic crystal growth (rod-like morphology). Moreover, adding Y_2O_3 promotes the crystallisation of the second phase (Figs. 6a, b). The TEM diffraction analysis shows that there are crystalline phases based on the Y_2O_3 composition such as $Si_3N_4.SiO_2.4Y_2O_3$, $Al_2O_3.2Y_2O_3$ at grain boundary areas. Also, the quantity EDS analysis of crystalline and amorphous regions confirms that there are Y-rich phases in the crystalline area (Fig. 7a, b). Crystallization of $Y_3Al_5O_{12}$ (YAG) minimizes the glass phase to improve high temperature mechanical properties. Conversely, addition of Al_2O_3 prevents the crystallisation of the second phase (Fig. 6b). It appears that the dissolved Al_2O_3 in the silicate phase stabilise the glassy intergranular phase and hinders crystallisation of the intergranular Y-Si-O-N liquid. A higher concentration of Al_2O_3 leads to a strength degradation. This degradation is due to a more equiaxed grain structure (Fig. 3: R8). Al_2O_3 tend to cause an unfavourable change in morphology from the idiomorphic rod-like to a more equiaxed grain structure.

c) Forming methods

The forming process as well as the proceeding powder preparation steps is very important in the manufacture of high temperature ceramics since defects introduced in these stages will normally remain in the product even after a successful sintering process. A forming technique such as pressing or cold isostatic pressing often causes defects in the final microstructure, particularly for the fine powder [6, 32]. We are interested in developing the samples by two methods of forming: dry compaction and slip casting (Table 4). The slip casting allows a higher density to be obtained (60-65%) in compared to dry compaction (50 - 55%). Slip casting show to be a suitable method for manufacturing parts from ultra fine powders [33-35].

Table 4. Densification of powder by different forming method

Forming method	Raw density (%D_{th})	Sintered density
(A) Slip casting	57.5	3.26
(B) Cold pressing	54.8	3.14
(C) Cold pressing + CIP	56.5	3.165
(D) Hot-pressed	-	3.26

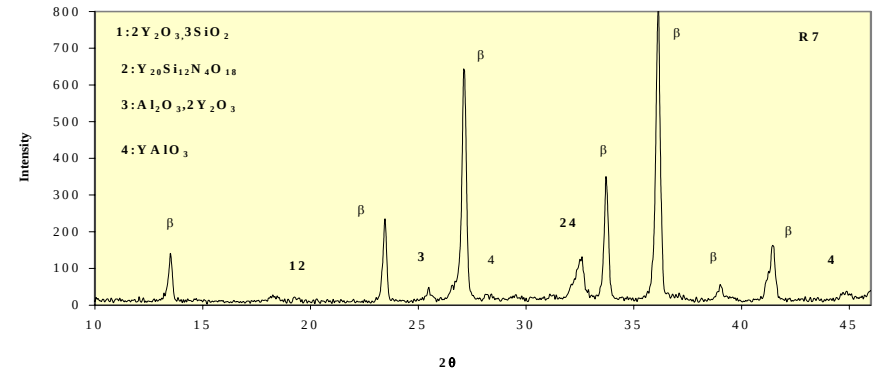

(a)

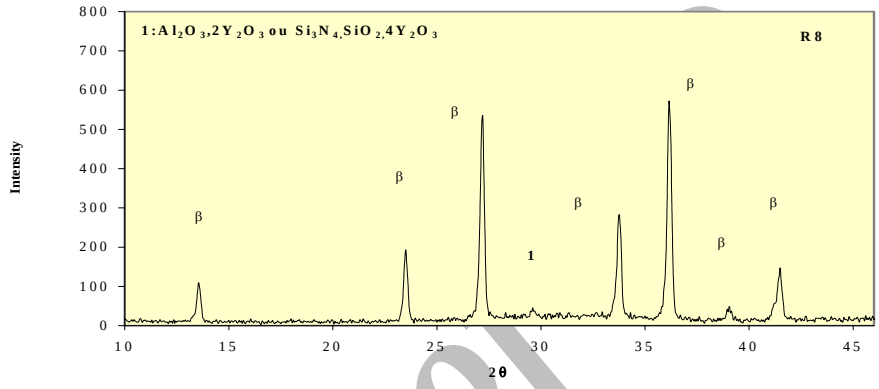

(b)

Fig. 6. X-ray pattern: Intensity as a function of diffraction angle 2θ (degrees) for materials, a) R7, b) R8

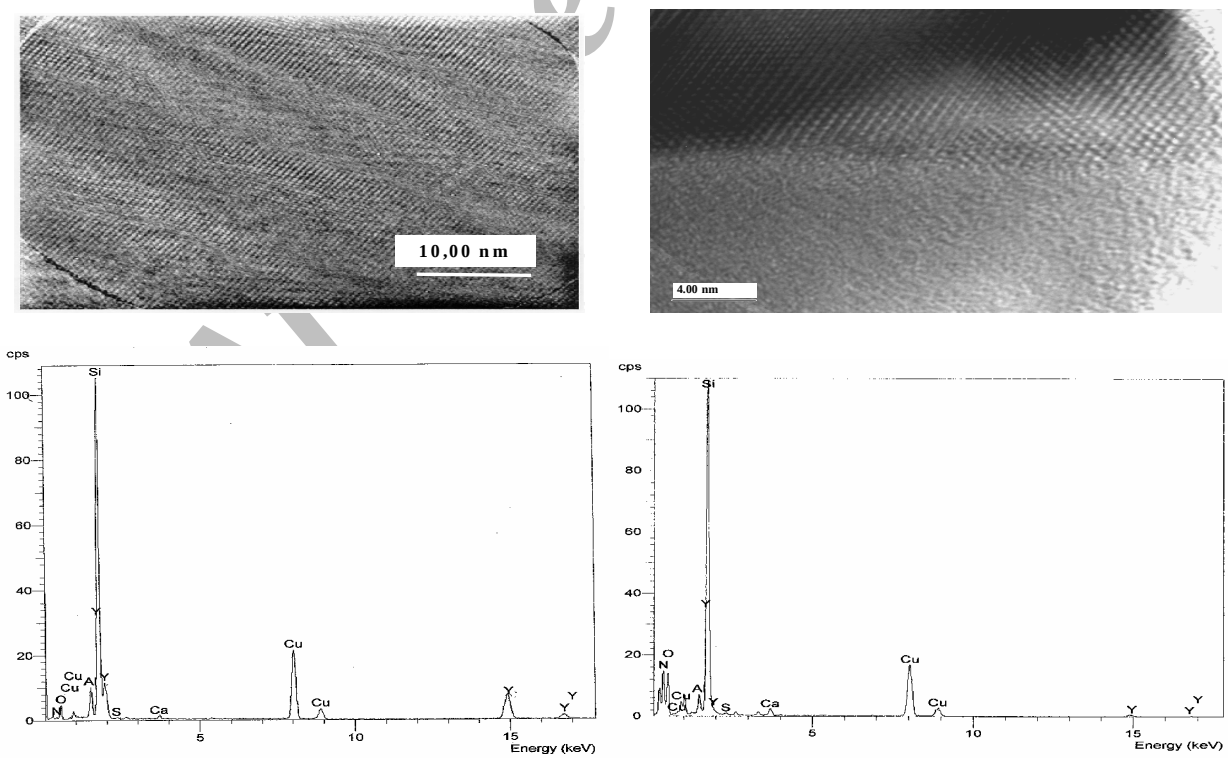

(a) (b)

Fig. 7. TEM micrographs of intergranular phase and EDS microanalysis for sample R8, a) crystalline area, b) amorphous area

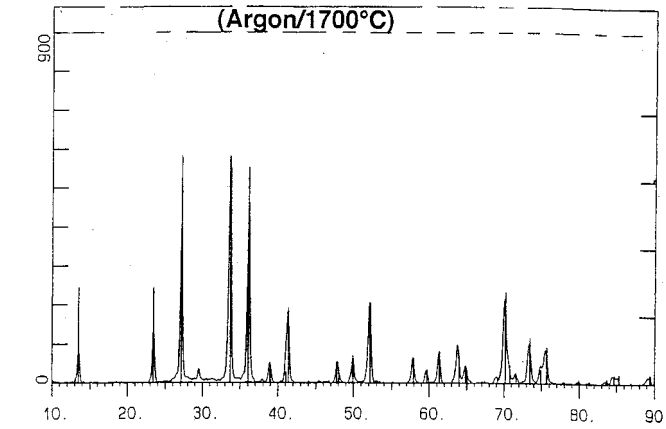

(a)

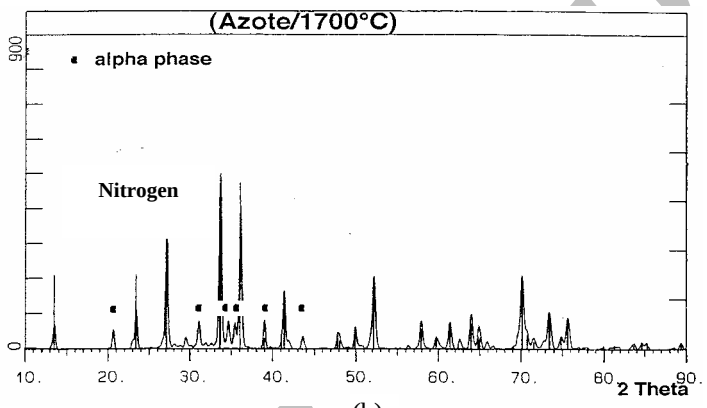

(b)

Fig. 8. X-ray pattern: Intensity as a function of diffraction angle 2θ (degrees) for materials, a) R1, b) R3

d) Sintering parameters

Atmosphere: The bulk density measurements show significant differences between samples treated under Nitrogen and Argon atmospheres (Table 3: R2, R4). The difference can be explained in terms of:

- The inhibitor effect of the Argon on the densification rate of the Si_3N_4.
- The presence of an atmosphere of Nitrogen that limits the decomposition of Si_3N_4 at the highest temperatures.

X-ray analysis reveals that atmosphere plays a significant role in $\alpha \rightarrow \beta$ transformation. Under an Argon atmosphere, the $\alpha \rightarrow \beta$ transformation is completed at 1700°C, while under nitrogen atmosphere it is completed only at 1800°C (Fig. 8a, b).

The SEM observation of the hot pressed samples under Argon shows large grain surrounded by a continuous amorphous intergranular phase, while at the same sintering condition, but N_2, the microstructures consist of smaller grains with a higher aspect ratio (prismatic β- grains) (Fig. 3: R2, R4) which result in better mechanical properties and thermal shock resistance (Table 3: R4).

Temperature and time: The higher sintering temperatures and the longer soaking time result in a decrease of porosity and therefore, increased densification. The temperature, however, is limited by the decomposition of Si_3N_4 and vaporisation of the liquid phase (>2000), although the density remains nearly constant for long soaking times.

The X-rays analysis reveals that the $\alpha \rightarrow \beta$ transformation is completed after 40 min at 1800°C, while the $\alpha \rightarrow \beta$ transformation is not completed at 1700°C, even after 60min (Table3: R12,R3). A rise in hot-pressing temperature results in a significant increase in the α to β transformation at a constant time. For

the hot pressed samples, the observation of the fracture surface by SEM shows an evolution of the microstructural development as a function of temperatures (Fig. 9a,b and c). At a higher temperature and longer soaking time, the microstructure changes in grain morphology to elongated grain. These microstructural changes result in an increase in flexural strength and fracture toughness and a higher thermal shock resistance (Table 3: R3, R4, R5). The reason for this is that the linked elongated β-crystals provide higher resistance to crack growth because of the absorption of energy, crack deflection and pull-out effects.

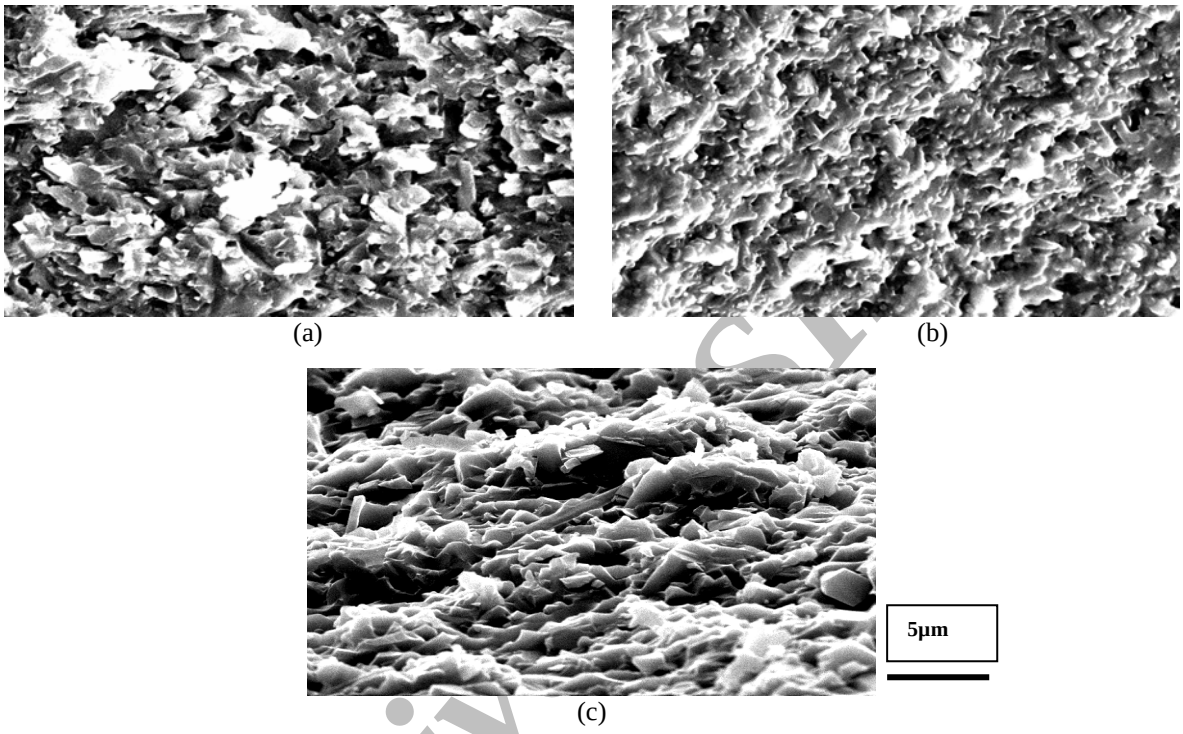

(a) (b)

(c)

Fig. 9. SEM fracture surface of a) R3, b) R4, c)R5

At a higher temperature than 1800 °C, increasing the isothermal holding time of sintering causes a lower strength level in association with higher impact toughness in the heat treated sample. This phenomenon is attributed to the larger eauiaxed grain size microstructure (Fig. 3: R17, R18), which needs a longer critical crack size to fracture. Moreover, the evaporation of the liquid phase and decomposition of Silicon Nitride cause a change in the analysis of the liquid phase. This effect is much higher in the SHS powder (Fig. 3: R21, R22) because of the heterogeneous distribution of particles and higher percentage of β-Si_3N_4.

Pressure: During hot pressing, the compacting behaviour of Si_3N_4 is also influenced by the application of the instant load. The point of load application (Fig. 10) at a higher temperature (T_d: dwell temperature) retarded a full compacting condition. In fact, the appearance of an interparticular phase hinders the particles rearrangement and flow. The load application at T_i avoids this event and the compacting behaviour becomes easier [36].

The load application at T_i increases the orientation effects in the microstructure more strongly than at T_d. This indicates a finer grain size with β-Si_3N_4 grains with high aspect ratios (fibrous morphology). This microstructure of self-reinforced Silicon Nitride shows a fracture toughness of more than 10 MPa.√m, a flexure strength of 800-900 MPa and a better R-curve (Fig. 11). For all the sintered samples by load application at T_i, the young's modulus is higher (Table 3).

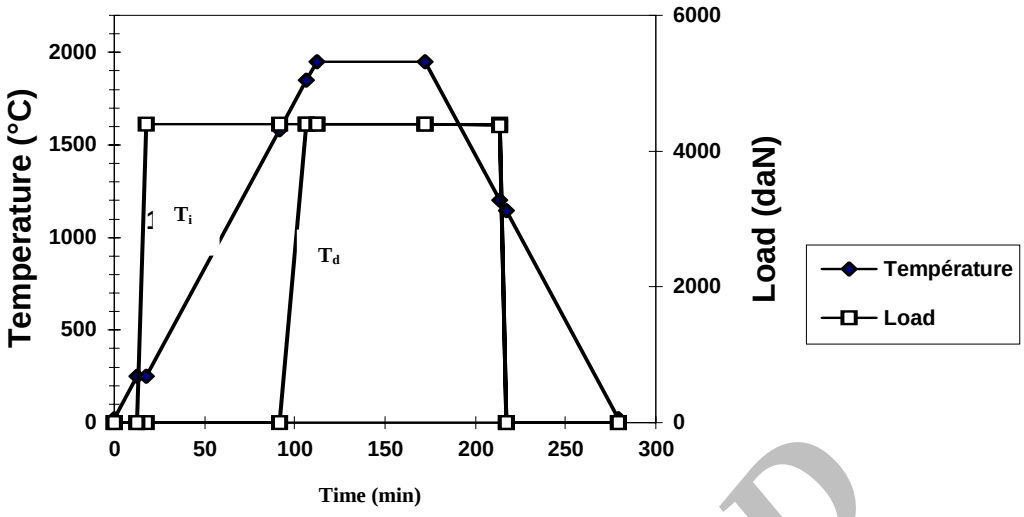

Fig. 10. Hot-pressed cycles of load and temperature

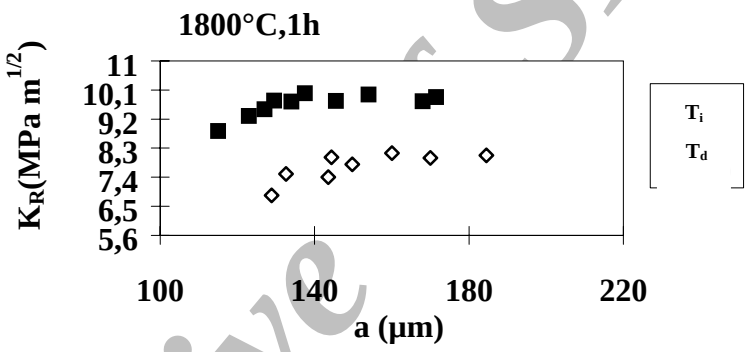

Fig. 11. R-Curve for sintered sample in different states of load application

e) Fabrication technique

The characteristics of materials resulting from slip casting plus sintered pressureless (A), cold pressing plus pressureless sintering (B) and hot pressed materials (C) are compared (Table 4). Materials of type A show a density comparable with that of the hot pressing (99.3%D_{th}). In fact, a high green density up to 65% for the slip-cast samples means a great sinterability of the samples prepared by slip casting due to more homogeneity of the particles rearrangement and the small quantity of the agglomerates. This makes it possible to better control the microstructural development during sintering, while materials of type B show low densification and mechanical properties (Table 3: R4, R13, R14). This can be noted by comparing the surface quality of materials sintered by three techniques (Fig. 12).

Hot pressing, the one process used some years ago with a simple shape and economic disadvantage, can be performed without additives at very high pressure (1.5 GPa). Pressureless sintering, meant to overcome the shape limitation and high production cost of hot-pressing, is carried out by liquid phase sintering using stable additives near of the atmospheric pressure in Nitrogen in order to avoid the decomposition of Silicium Based Ceramics.

The mechanical characteristics of slip-cast materials are comparable with those of materials fabricated by hot pressing. The fracture toughness, the curve R and thermal shock resistance are higher than that of hot pressing (Figs. 13a, b). The slip casting sample contains a uniform microstructure, particularly the

small pores with uniform distribution (finer voids of approximately of 1-2 μm in size and nearly spherical in shape) compared to hot pressed samples (Fig. 3: R19, R20).

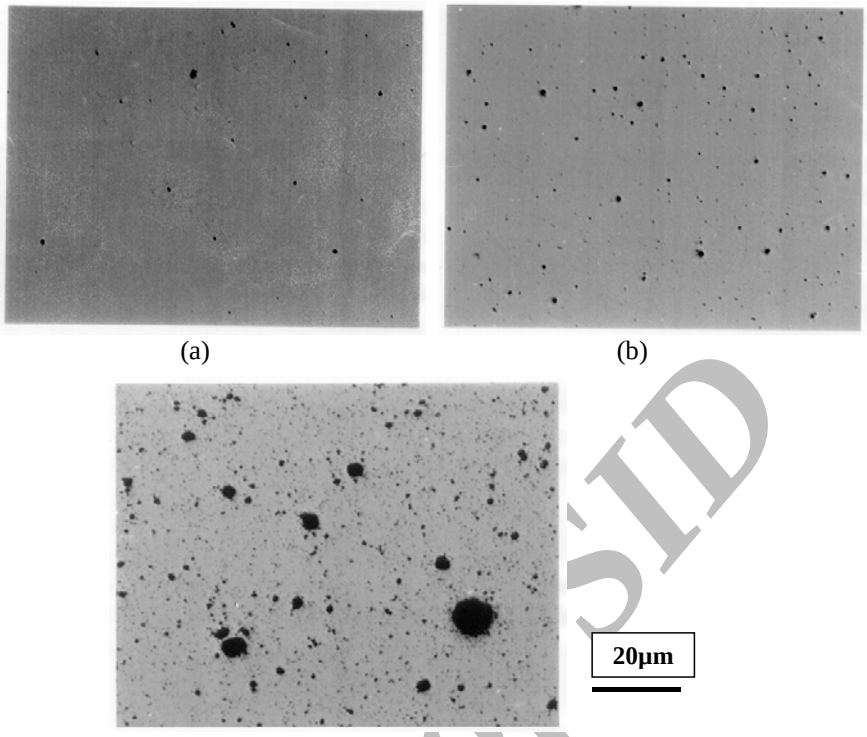

Fig. 12. Optical photographic of the sintered samples in a)Hot-pressing b) Slip casting c) cold pressing

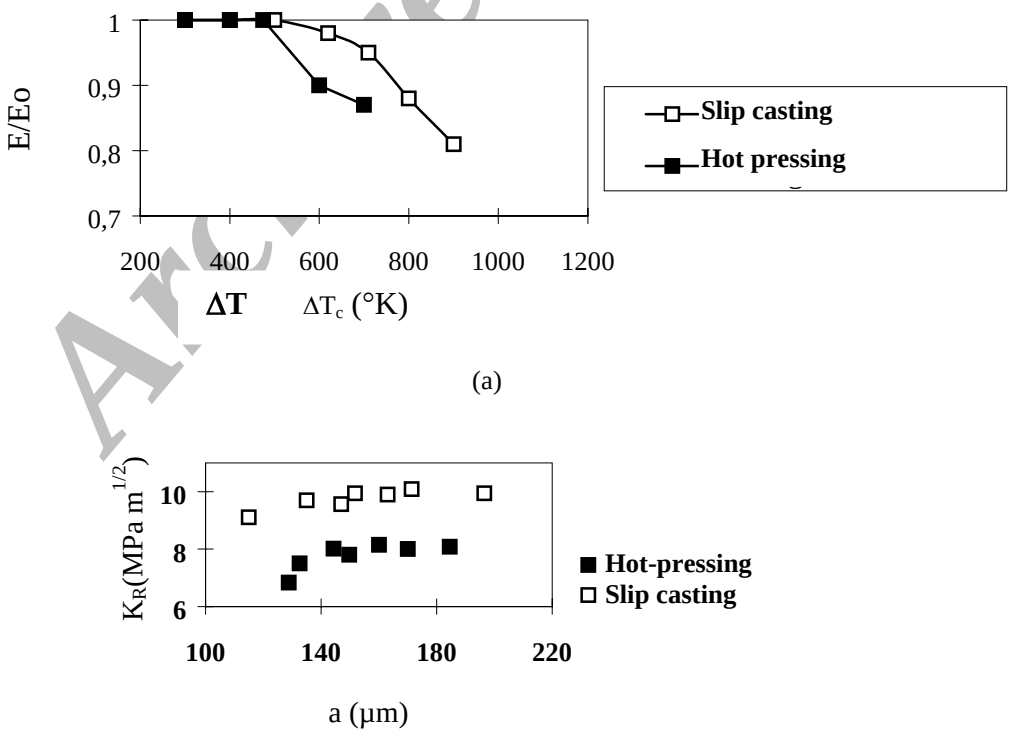

Fig. 13. a) ΔT_c changment and b) the effect of curve R for sintered Silicon Nitride in 1800°C during 1 hour by two different techniques of fabrication

In slip cast bodies, failure origins are predominantly from voids in the form of bubbles under the surface. In our case, we have machined a good thickness to give a higher strength.

It is necessary to notice that for the slip-cast samples, the heating rate must be slow in spite of a heat treatment before sintering. In our experiment, the blow thermal cycles sintering give a better result on the densification:

1) 1) 25 $\rightarrow$ 500°C: $V_{heating}$ = 4°/min, under vacuum
2) 500°C: $t_{holding}$ =20 min, P=1atm (N_2)
3): 500 $\rightarrow$ 1200 °C $V_{heating}$ =10°/min
4) 1200$\rightarrow$1800°C $V_{heating}$ =15°/min
5) 1800°C : $t_{soaking=}$ 60 min.

f) Post sintering

For sample R20, a supplementary heat treatment process called ″post-sintering″ was carried out at 1700 °C using a 500 bar isostatic hot pressing under a Nitrogen control condition. A significant decrease in the porosity (1.2% to 0.2%) and so an increase in the density of the sample (98.1% to 98.7%) was observed as a result of this process. The fracture strength is increased from 714 to 800 MPa, but the impact toughness is decreased from 9.4 to 6 MPa $m^{-1/2}$. One of the reasons for the lower impact toughness is a finer microstructure which needs a shorter critical crack size to be brittle (Fig. 14). Therefore, post–sintering is not a good heat treatment process to increase the impact toughness.

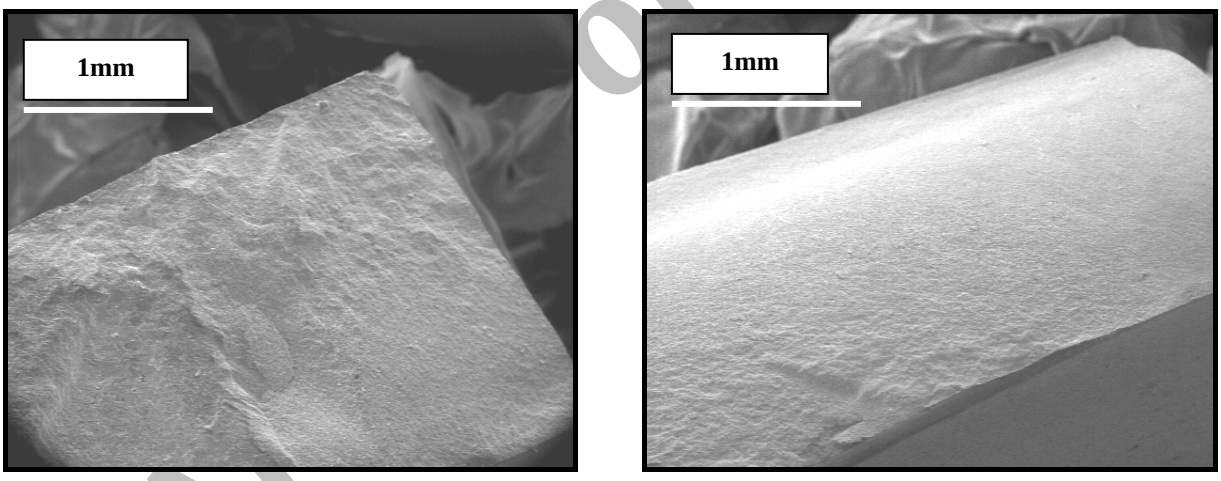

Fig. 14. Comparison of the fracture surface for samples a) before post sintering b) after post sintering

4. CONCLUSION

•The powder SN-E10 with a high percentage of α-phase ≥97%, equiaxial particle morphology and a lower particle size results in a rod-like morphology and higher mechanical properties than M11 or S.H.S and a maximum value of ΔT_c (870°C)

•The higher amount of Y_2O_3 results in an increase in viscosity so that a saturated state of melt is kept and helps the crystallisation of grains with high aspect ratios. Furthermore, Y_2O_3 helps the crystallisation of the second phase and decrease the amount of the glassy phase, but AL_2O_3 prevents this effect. These characteristics of Y_2O_3 result in a high amount of ΔT_c of 850°C. The higher concentration of Al_2O_3 results in the modification of microstructure with a more equiaxed grain.

•The slip casting process in relation to powder metallurgy results in a higher density, fracture toughness and thermal shock resistance.

•At a higher sintering temperature (2000°C) and longer soaking times (1h), microstructure changes in grain morphology toward elongated grain that results in an increase in mechanical properties and a higher thermal shock resistance.

•Atmosphere plays a significant role in the a) $\alpha \rightarrow \beta$ transformation, b) Bulk density and c) grain morphology. N_2 atmosphere results in higher densification and a microstructure with a higher aspect ratio and finer grain size and a higher amount of β phase.

•The load application at the beginning of the thermal cycle (T_i) in comparison with application at the beginning of 1^{st} dwell temperature (T_d) strongly increases the orientation of the microstructure, while decreasing the grain size (self-reinforced Si_3N_4) which results in the mechanical properties of $Ki_c \geq 10MPam^{\sqrt{2}}$ and $\sigma_f \geq 900MPa$ and higher thermal shock resistance (800°C).

REFERENCES

1. Lange, F. F. (1983). Fabrication and properties of dense polyphase silicon nitride. *Ceramic Bulletin, 62*(12), 1369-74.
2. Riley, F. L. (1985). Production, properties and application of silicon nitride ceramics. *World Ceramics, 22*, 85-90
3. Suematsu H., Mitomo, M., Mitchell T.E., Perrovic J., Fukunage & Ohashi, N. (1997). The α−β transformation in silicon nitride single crystals. *J. Am. Ceram. Soc., 80*(3), 615-620.
4. Shimada, M., Tanaka, A., Yamada, T. & Koizumi, M. (1983). Densification and phase transformation of SI3N4 by high pressure sintering. Ceramic powders edited by P. Vincenzini, Amesterdam, Elsevier Scientific, 871-79.
5. Wotting, G., Kanka, B. & Ziegler, G. (1985). Microstructural development, micostructural characterisation and relation to mechanical properties of dense silicon nitride. *Fortschrittsber, DKG*(1), 83-96.
6. Bellosi, A., Galassi, C., Roncari, E., Fabbriche, D. D. & Capiani, C. (1986). Production of Si3N4 base materials. *Science of ceramic,14*, 151-56.
7. Mieskowski, D. M. & Sanders, W. A. (1989). Hot isostatic pressing of silicon nitride with boron nitride, boron carbide, and carbon additions. *J. Am. Ceram. Soc., 72*(5), 840-843.
8. Martorana, A. D. & Silengo, B. (1977). Some consideration on the kinetic of hot-pressing Alpha-silicon nitride powder. *Mater. Sci. and Eng., 28*, 215-220.
9. Ziegler, G., Heinrich, J., Wotting, G. (1987). Relationships between processing, microstructure and properties of dense and reaction-bonded silicon nitride. *J. Mater. SC., 22*, 3141-86.
10. Wotting, G. & Ziegler, G. (1986). Powder characteristics and sintering behaviour of SI3N4-powder. *Powder Metallurgy International, 18*(1), 25-31.
11. Lee, H. J. & Yoshida, T. (1996). Microstructures of ultrafine SI3N4 powder compacts induced by rapid heating under controlled thermograms. *J. Mater. SC., 31*, 1647-1651.
12. Hirosaki, N., Okamoto, Y., Akimune, Y., Isozaki, K. & Mitomo, M. (1995). Effect of purification of β-SI3N4 powder on the strength of sintered materials. *J. Ceram. Soc. Japon,103*(6), 630-634.
13. Mitomo, M., Yang, N., Kishi, Y. & Bando, Y. (1988). Influence of powder characteristics on gas pressure sintering of SI3N4. *J. Mater SC., 23*, 3413-3419.
14. Lee, W. E. & Rain, W. M. (1994). *Ceramic microstructures property control by processing*. University Sheffield U.K, 29-70.
15. Olagnon, C. (1990). Influence des conditions d'élaboration sur la microstructure et les propriétés mécaniques du nitrure de silicium. Thèse Doctorat, Institut National des Science Appliquées de Lyon-France, 140.
16. Wotting, G. & Ziegler, G. (1983). Microstructural development of sintered, hot-pressed and hot isostatic-pressed silicon nitride. Science of ceramics, *12*, 412-424.

17. Zutshi, A., Haber, A., Niez, E., Adams, W., Wachtman, B. (1994). Processing microstructure, and wear behavior of silicon nitride hot- pressed with alumina and yttria. *J. Am. Ceram. Soc., 77*(4), 883-890.
18. Hirosaki, N. & Akimune, Y. (1993). Effect of grain growth of β-silicon nitride on strength, weibull modulus, and fracture toughness. *J. Am. Ceram. Soc., 76*(7), 1892-1894.
19. Hirao, K., Nagaoka, T., Brito, M. E. & Kanzaki, S. (1996). Mechanical properties of silicon nitride with tailored microstructure by seeding. *J. Ceram. Soc*. Japan, *104*, 55-59.
20. Li, C., Lui, S. & Goldacker, J. (1982). Relation between strength, microstructure, and grain-bridging characteristics in situ reinforced silicon nitride. *J. Am. Ceram. Soc*., *65*(1), 449-459.
21. Yzik, A. J. & Beaman, D. R. (1993). Microstructure and properties of self-reinforced silicon nitride, *J. Am. Ceram. Soc.*, *76*(11), 2737-2744.
22. Galik, P., Dusza, J. & Hoffmann, J. (1995). Relation between microstructure, toughening mechanisms, and fracture toughness of reinforced silicon nitride ceramics. *J. Am. Ceram. Soc., 78*(10), 2619-2624
23. Ziegler, G., Heinrich, G. & Wotting, G. (1987). Relationships between processing, microstructure and properties of dense and reaction-bonded silicon nitride. *J. Mat. Sc., 22*, 3041-3086.
24. Mulla, M. A. & Krstic, V. D. (1991). Low temperature pressureless sintering of β-SiC with Aluminium oxide and yttrium oxide additions. *Ceramic Bulletin, 70*(3), 439-443
25. Hirosaki, N., Okada, A. & Matoba, K. (1988). Sintering of SI3N4 with the addition of Rare-earth oxides. *J. Am. Ceram. Soc., 71*(3), C-144_C-147.
26. Wedel, M. K., Falk, L. K. L. & Ekstrom, T. (1992). Characterisation of SI3N4 ceramics formed with different oxide additive. *J. Hard Material*, *3*(3-4), 435-445.
27. Sanders, W. A. & Mieskowski, D. M. (1985). Strength and microstructure of sintered SI3N4 with rare-earth-oxide additions. *J. Am. Ceram. Soc. BULL., 64*(2), 304-309.
28. Dutta, S. & Buzek, B. (1984). Microstructure, strength, and oxidation of a 10 wt% Zyttreite-SI3N4 ceramic. *J. Am. Ceram. Soc., 67*(2), 89-92.
29. Lagarde, T., Pelletier, J. & Arnal, Y. (1999). Parametric study of the etching of SiO_2 in SF_6 plasmas: Modeling of the etching kinetics and validation. *J. Vac. Technol., B17*(1), 1-9.
30. Chevalier, J. (1996). Etude de la propagation des fissures dans une zircone 3Y, TZP pour application biomedicales. Thèse Doctorat, Institut National des Science Appliquées de Lyon-France, 161.
31. Chevalier, J., Olagnon, C. & Fantozzi, G. (1996). Study of residual stress field around Vickers indentation in a 3Y- TZP. *J. Mat. Sci., 31*, 2711-2717.
32. Lang, F., Colic, M., Frank, G. & Fisher, M. (1998). *Plastic forming of silicon nitride powder via colloidal processing*. Materials department, University of California.
33. Torre, J. P. & Bigay, Y. (1986). Fabrication of silicon nitride parts by slip casting. *The ceramic Engineering and Science Proceeding, 7*(7-8), 890-897.
34. Hartmann, W. J. A. M. & Van Dijen, F. K. (1986). Slip casting parameters for commercial Si_3N_4 powders. *Journal de physique, 47*(2-8), C1-79.
35. Abinovich, E. M. & Leitner, S. (1982). Slip casting of silicon nitride for pressureless sintering, *J. of materials science, 17*, 323-328.
36. Schubert, C., Pabst, J. & Klein, U. (1989). Computer aided evaluation of the silicon nitride hot pressing compaction process. cfi/Ber. DKG, *66*(10), 420-24.